RISET

Geologi dan Pertambangan
Indonesian Journal of Geology and Mining

https://jrisetgeotam.lipi.go.id

Research article

Modeling of individual debris flows based on DEMNAS using Flow-R: A case study in Sigi, Central Sulawesi

Corresponding author:
Moch Hilmi Zaenal Putra
E-mail address: mochhilmizp@gmail.com

Moch Hilmi Zaenal Putra[1,3], Indra Andra Dinata[2], Imam Achmad Sadisun[2], Dwi Sarah[3], Atin Nur Aulia[3], Sukristiyanti[3,4]

[1]Master Degree Program in Geological Engineering, Faculty of Earth Sciences and Technology, Institute of Technology Bandung (ITB), Bandung, Indonesia
[2]Faculty of Earth Sciences and Technology, Institute of Technology Bandung (ITB), Bandung, Indonesia
[3]Research Center for Geological Disaster, National Research and Innovation Agency, Bandung, Indonesia
[4]Doctoral Degree Program on Geodesy and Geomatics, Faculty of Earth Sciences and Technology, Institute of Technology Bandung (ITB), Bandung, Indonesia

ABSTRACT On 2018 September 28, 18:03 a local time (10:03 am UTC), the Mw 7.5 earthquake with a focal depth of about 20 km devastated the Palu region in Central Sulawesi, Indonesia resulting in a catastrophic disaster and many casualties. The Palu earthquakes triggered widespread landslides upstream, contributing to the sizeable material volume accumulated in rivers and mountain slopes. After the Palu earthquake, from September 28, 2018, until December 2021, at least 24 events of debris floods have occurred, which have spread to 15 villages. As of late, the empirical debris flow model Flow-R, software for susceptibility mapping of debris flows at a regional scale, was published. While Flow-R's applicability on a regional scale has been confirmed in several studies, the calibrated case using back-analysis of individual debris flow events in Indonesia based on DEMNAS with a spatial resolution of 8.3 m has never been conducted. Local debris flows modeling using Flow-R was evaluated with three well-documented debris flow events on the break slopes on the west and east sides of the Palu Valley. Quantitative analysis was carried out in this study to assess the accuracy, positive predictive value, and negative predictive value of models. First, the result shows the individual back-analysis model of debris flows found good agreement between debris-flow paths predicted and documented debris flow path extent. However, the parameters for rheological properties and erosion rate required in the software are limited. Second, the quantitative analysis shows accuracy, positive, and negative predictive value, which varies considerably. Based on the study, Flow-R is not suitable for comprehensive hazard mapping but provides a direct information about possible run-outdebris flow paths. Furthermore, lateral spreading and friction of Flow-R model results can be used to calibrate the process with rheological properties and erosion rate in other numerical modeling software, either for forward or back analysis.

INTRODUCTION

On numerous alluvial fans, urban settings have replaced natural areas, which had been the space of stream channel meandering, sedimentation areas, and lessening of flow energy. Due to the highly lengthy intervals between these events, little consideration had been paid to these regular cycles, bringing about a mistaken feeling of safety from damaging floods before the newcomers were confronted with the flooding issue. Each stage in the urban development and infrastructure produces an irreversible situation without leaving the entire expanse for the section of floods and their sediments. Ideal planning for debris flows or debris floods protection became progressively troublesome.

Alluvial fans in Venezuela, Los Angeles, and lesser-known areas, for example, Palu, and Ambon are sites episodic of rainfall-induced natural hazards. Debris flows and debris floods that occur episodically in these alluvial fans lead to numerous high-risk residents during intense and prolonged rainfall. The case of debris flood and debris flow in Vargas State, Venezuela in 1999 (Larsen et al., 2001) and Ambon, Indonesia, in 2012 (Ishizuka et al., 2017) showed a massive damage impact. It resulted in numerous casualties in a densely populated alluvial fan environment. Although scientists have improved their ability to identify areas of high natural hazard, population growth and development pressure have put more people at risk.

Debris flow hazard modeling was developed in the previous years to assess debris-flow hazards. The empirical debris flow model Flow-R (Flow path assessment of gravitational hazards at a regional scale) was published, software for susceptibility mapping debris flows at a regional scale. It allows the propagation extent, basically based on a DEM (Digital Elevation Model). Flow R has been proved to generate regional debris flow susceptibility maps with satisfying accuracy. Even though Flow-R is not explicitly intended for debris-flow modeling on a local scale, it is suggested to compare the assessed susceptible zone with specific events to evaluate the accuracy of the results (Horton et al., 2013). Individual events have been compared on highly resolution DEM (2 m). The result showed that the accuracy, positive predictive value, and negative predictive value of Flow-R modeling could reach 0.8, 0.8, and 0.9, respectively (Fischer et al., 2016). However, a comparison of individual debris flows events in Indonesia based on DEMNAS (Digital Elevation Model Nasional) with a spatial resolution of 8.3 m has never been conducted. Therefore, the assessment accuracy of Flow-R on a local scale is the main objective of this study. It is hypothesized that when applied to the recommended digital elevation model resolution, i.e up to 10 m (Horton et al., 2013), the Flow-R represents a sophisticated hydraulic model in modeling individual debris flow events. This hypothesis was tested concerning the three affected areas in Sigi, Central Sulawesi.

STUDY AREA

Geological Setting

Morphology of the Palu Valley area in Palu-Sigi is characterized by a ten km-wide lowland and mountains trending N-S on both east and west, reaching an elevation of 2.3 km. The valley's lowland is considered a pull-apart basin created by the Palu–Koro Fault (Bellier et al., 2006, 2001; Socquet et al., 2006).

Overall, the study area covers the Palu watershed which can be divided into 72 sub-watersheds, 36 on each west and east sides (**Figure 1**). DEMNAS is used for watershed delineation in this study by the hydrological module of QGIS software. The residential area is distributed mostly on the west side of Sigi Regency, which is close to the break of slope and sediment source.

The high mountains dominantly consist of metamorphic complexes and granitic rocks that are Latimojong formation (Kls), granite intrusive rocks (Tmpi), and metamorphic complex (Km) (Simandjuntak et al., 1997; Sukamto et al., 1973; Sukido et al., 1993) (**Figure 2**). Holocene deposits, mostly alluvial fan deposits, cover the lowland along the Palu River. Clastic rock elements from the steep topography on both the east and west sides of the river generate several small to large alluvial fans that spread from a confined valley to a nonconfined lowland area.
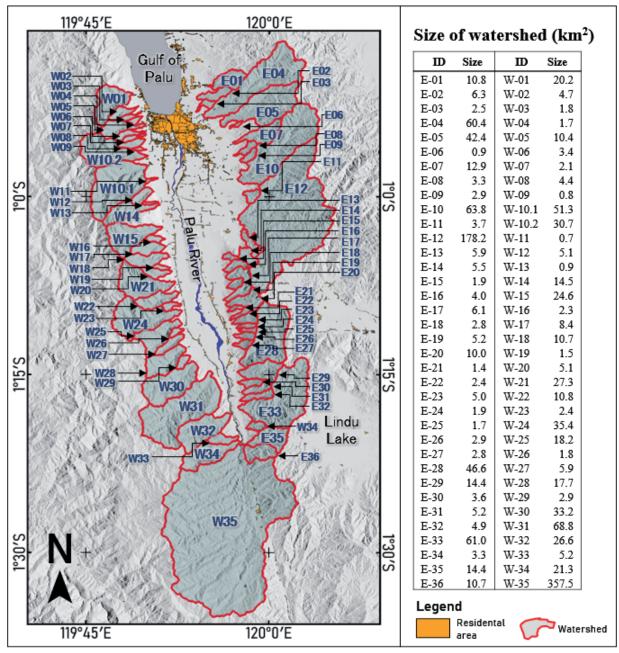

Figure 1. Distribution of the Palu sub-watershed which is divided into 72 units; red polygons represent the distribution of the residential area.
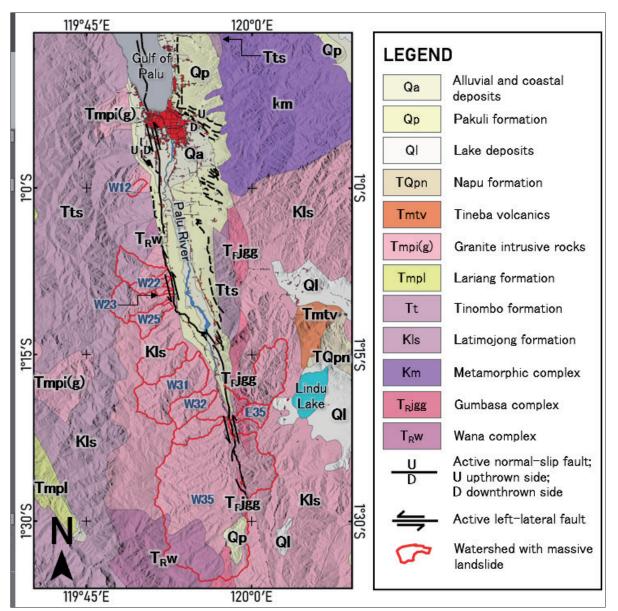
Figure 2. Distribution of watershed, active faults (Natawidjaja et al., 2021), and lithology (Simandjuntak et al., 1997; Sukamto et al., 1973; Sukido et al., 1993) around The Palu Valley, Central Sulawesi.

Palu's Earthquake

On 2018 September 28, 18:03 a local time (10:03 am UTC), the Mw 7.5 earthquake with a focal depth of about 20 km (USGS, 2018) devastated the Palu region in Central Sulawesi, Indonesia, resulting in a catastrophic disaster and a large number of casualties. Along the eastern edge, there are numerous normal faults. It cut through Quaternary deposits, causing some to rupture during the 2018 event (Natawidjaja et al., 2021; Patria and Putra, 2020). Palu earthquakes trigger widespread landslides on many scales in more than 70 hilly locations in Palu, Sigi, and Donggala(Sukatja et al., 2021). A slope is caused to become unstable by the inertial loading or by causing a loss of strength in the slope materials. The red watershed polygon (W12,W21, W22, W23, W24, W25, W30, W31, W32, W34, W35, E33, and E35) showed the watershed distribution with massive landslides after the Mw 7.5 Palu Earthquake on September 28, 2018 (**Figure 2**). We also provide the images extension files of the waterhed with massive landslide in the e-Supplement (Figure S1 - S13).

Debris Flow and Debris Flood Disaster

Alluvial fan morphology found in Sigi, Central Sulawesi, indicates that the area is susceptible to geological hazards such as debris flows and floods. The Palu earthquake of September 28, 2018, significantly contributed to the criticality of upstream slopes and the large volume of material accumulated in rivers and mountain slopes. The rainy season of La Nina triggers debris avalanches on the slopes, transforming into the debris flow, hyper-concentrated flow, and debris flood. After the Palu earthquake, from September 28, 2018, until December 2021, at least 24 events of debris floods and debris flows have occurred, which have spread to 15 villages (**Table 1**). Based on National Agency for Disaster Management (2021)report, all of them were triggered by high and prolonged rainfall.

Table 1. List of debris flood events in the Palu Valley after the Palu earthquake from 28 September 2018 to December 2021(National Agency for Disaster Management, 2021)

No.	Location	WS	Date	Fatalities		Damaged house			Facilities
				Death	Affected	Heavy	Moderate	Light	
1	Bangga, Dolo Selatan	W31	16/11/2018	0	701	0	0	196	0
2	Salua, Kulawi	E35	11/12/2018	0	427	0	81	0	2
3	Omu, Gumbasa	E33	17/02/2019	0	53	0	0	0	1
4	Omu, Gumbasa	E33	25/02/2019	0	7	0	0	0	0
	Walatana, Dolo Selatan	W30		0	237	0	0	0	0
	Balongga, Dolo Selatan	W22		0	185	0	0	0	5
5	Bangga, Dolo Selatan	W31	28/04/2019	1	1952	0	0	0	7
	Omu, Gumbasa	E33		0	92	0	0	0	0
	Tuva, Gumbasa	E33		0	342	0	0	0	2
6	Namo, Kulawi	W35	13/08/2019	0	215	10	0	40	3
7	Poi, Dolo Selatan	W23	08/12/2019	0	39	5	0	7	0
8	Bolapapu, Kulawi	W35	12/12/2019	2	390	11	19	75	0
9	Sungku, Kulawi	W35	06/04/2020	0	39	0	0	0	0
10	Omu, Gumbasa	E33	26/04/2020	0	74	0	0	0	2
	Tuva, Gumbasa	E33		0	0	0	0	0	1
11	Poi, Dolo Selatan	W23	27/04/2020	0	74	6	0	0	0
12	Sungku, Kulawi	W35	06/05/2020	0	39	0	0	0	0
13	Sambo, Dolo Selatan	W21	08/05/2020	0	0	0	0	0	0
14	Tuva, Gumbasa	E33	12/05/2020	0	0	0	0	0	0
15	Poi, Dolo Selatan	W23	15/05/2020	0	85	2	0	15	0
16	Omu, Gumbasa	E33	18/06/2020	0	0	0	0	0	0
17	Oloboju, Sigi Biromaru	E12	09/07/2020	0	0	2	0	3	0
	Sidera, Sigi Biromaru	E12		0	0	0	0	0	0
18	Bolapapu, Kulawi	W35	08/08/2020	0	473	18	2	3	2
19	Walatana, Dolo Selatan	W30	06/09/2020	0	112	0	0	2	0
20	Oloboju, Sigi Biromaru	E12	08/09/2020	0	16	0	3	0	0
	Sidera. Sigi Biromaru	E12	08/09/2020	0	16	0	3	0	0
21	Rogo, Dolo Selatan	W25	14/09/2020	0	176	13	60	2	0
22*	Beka, Marawola	W12	27/03/2021	0	0	2	75	215	0
23*	Rogo, Dolo Selatan	W25	30/08/2021	0	179	5	0	0	2
24*	Salua, Kulawi	E35	10/10/2021	0	49	4	9	12	0

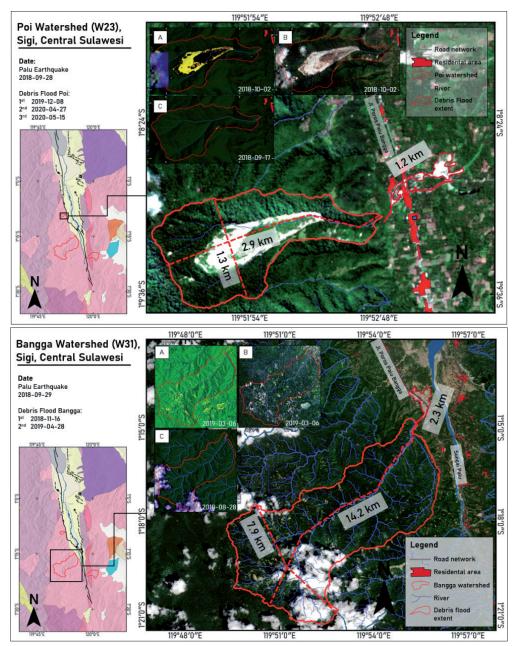Note: *additional input based on search results in online media

WS: watershed

METHOD

Mapping the Source Area

Mapping the source area and area using a scripting facility has been made by Ariza and Davila (2021) to detect landslides using space-based data in Sentinel Playground and EO Browser. The script for erosion detection for rapid mapping is based on the response of the Barren Soil Index BSI to detect recent traces of soil movement.

The results are shown in an R:G:B composite image, with yellow representing surficial soils or debris slides. Source area mapping was carried out in Poi, Bangga, and Salua Villages representing well-documented debris flow events on the break slopes on the west and east sides of the Palu Valley. Three events were selected for evaluation that is debris flood events in Poi Village (W23 ~2.4 km², 2019-2020 event), Bangga Village (W31 ~68.8 km², 2018-2019 event), and Salua Village (E35 ~14.4 km², 2018 & 2021 event). Sentinel 2 image taken after Palu Earthquake events in upstream (**Figure 3.B**), comparing spectral indexes on bare soils after (**Figure 3.A**) and before (**Figure 3.C**) Palu Earthquake event.

Figure 3. Map showing coverage of Poi (23/06/2020), Bangga(05/11/2020), and Salua(28/08/2019) Watershed. A, B) Barren soil index and natural color several days after Palu Earthquake showed massive debris avalanches and debris flows upstream; C) Barren soil index several days before Palu Earthquake.

Debris Flow Modelling

A Digital Elevation Model and a raster file with the source areas prepared in any GIS software are the required input data. The topography on which the flow propagates is depicted by the Digital Elevation Model, which must be in raster format. The source area file is a raster file that contains the sources of a mass movement, which form the starting cells of the propagation of the flow. The lateral spreading and friction models are two types of algorithms used in the propagation assessment.

The lateral spreading algorithm controls the path and spread of debris flow controlled by the flow direction algorithm and persistence function. The modified version of Holmgren's was chosen for modeling. It is becausethe algorithm improved the spreading extent by making it less sensitive to DEM small features and thus less reliant on DEM resolution. It provides more realistic coverage and allows for more accurate spreading in flat areas such as alluvial fan morphology in the studied area. Holmgren's modified algorithm (Horton et al. 2013) represented in **Equation 1** is a modification of the algorithm from Holmgren (1994)in which the gradient value is changed by adding an extra height of dh to the center cell.Where i, j are the flow directions, p_i^{fd} is the susceptibility proportions in direction i, $tan\beta_i$ is the slope gradients between the central cell and the cell in direction i, and x is the variable exponents. The algorithm from Holmgren (1994) is based on a Multiple flow direction algorithm(Quinn et al., 1991), but adds an exponent x to control the flow divergence. The spreading direction for x = 1 is the same as the multiple flow direction. When x increases, the divergence decreases until it reaches zero, resulting in a single flow direction.

$$p_i^{fd} = \frac{(tan\beta_i)}{\sum_{j=1}^8 (tan\beta_j)^x} \ \forall \begin{cases} tan\beta > 0 \\ x \in [1; +\infty[, \end{cases} \quad (Eq.1)$$

The friction models algorithm determining the run-out distance would be able to reach based on its energy (**Equation 2**). Where E_{kin}^i is the kinetic energy of the cell in direction$i$, E_{kin}^0 is the kinetic energy of the central cell, ΔE_{pot}^i is the change in potential energy to the cell in direction$i$, E_f^i is the energy lost in friction to the cell in direction i. As the source mass is unknown, the energy balance is unitary.

$$E_{kin}^i = E_{kin}^0 + \Delta E_{pot}^i - E_f^i \quad (Eq.\,2)$$

To determine the maximum runout distance of a mass movement, the travel angle or Simplified Friction-Limited Model (SFLM) was used. It is the angle formed by the line connecting the source area to the farthest point reached by the mass movement that is based on a minimum travel angle (TA) (**Equation 3**) and maximum velocity (vlim) (**Equation 4**). The other friction model developed by Perla et al. (1980) is similar to the one developed by Voellmy (1955) and was designed for snow avalanches that did not occur in the studied area. As a result, SFLM was chosen for friction algorithm parameters rather than Perla et al. (1980). A mass movement in a steep catchment can reach unrealistic velocities during propagation, resulting in improbable run-out distances. The SFLM employs a velocity threshold to ensure that realistic velocities are not exceeded, resulting in more realistic run-out distances. The smaller the travel angle (TA) and the higher the maximum velocity (vlim), the further the run-out distance.

$$E_f^i = g\Delta x \tan\varphi \quad (Eq.\,3)$$

where E_f^i is the energy lost in friction from the central cell to the cell in direction i, Δx the increment of horizontal displacement, φ the travel angle in degree, and g the gravitational acceleration.

$$v_i = \min\left\{\sqrt{v_0^2 + 2g\Delta h - 2g\Delta x \tan\varphi}\,,\, v_{max}\right\} (Eq.\,4)$$

where v_i is the velocity at the end of the segment i, v_0 the velocity at the beginning of the segment, Δh the difference in elevation between the central cell and the cell in direction i, Δx the increment of horizontal displacement, φ the travel angle, g the gravitational acceleration, and v_{max} the given velocity limit.

The operation of the debris flow model was carried out on the DEMNAS with a spatial resolution of 8.3 m. This resolution was chosen since it is the highest resolution that covers the full research area and is readily available. The type of modeling is a back analysis, then an iterative debris flow modeling process is adjusted until the output obtained fits the observed debris flow extent as well as possible (**Figure 4**).
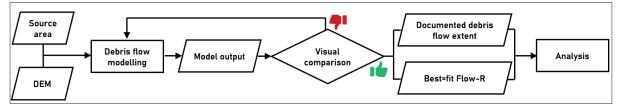

Figure 4. Research design flowchart for assessing the application of Flow-R in local debris flow modeling.

Flow-R is a spatially distributed empirical model developed in Matlab® for the propagation modeling of mass movements at the regional scale. The susceptibility is based on different propagation possibilities, not just on a single event. Flow-R has a user-friendly graphical user interface (GUI) that allows non-experts users to define source area delineation criteria, algorithms, and parameters for propagation assessment without requiring expert knowledge of complicated models (**Figure 5**). The type of modeling is a back analysis, then iterative debris flows modeling process by adjusting the parameter value (i.e.dh, x, weight, angle, and velocity values) until the output obtained fits the observed debris flow extent as well as possible.

	Parameter	Unit
Lateral spreading (Holmgren modified)	The extra height (dh): the extra height added to the central cell	m
	Spreading exponent (x)	-
Friction model (Simplified Friction-Limited Model or SFLM)	Travel angle (TA): specify the angle of reach	Degrees (°)
	Limit velocity (vl_{lim}) limits the specified maximum flow velocity	m/s

Figure 5. Flow-R's main user interface is equipped with a user-friendly graphical user interface (GUI).

Evaluation of Flow-R modeling

Quantitative analysis using Begueria'sconfusion matrix methodology was carried out in this study to assess the accuracy or predictive power (Beguería, 2006). This analysis was performed by comparing the model output (prediction) of Flow-R with the documented events of debris flow. The resulting matrix of intersection rates between model outputs and documented events is divided into four classes: TP (True Positive), TN (True Negative), FP (False Positive), and FN (False Negative) (**Figure 6**). In **Figure 6**, some statistics are commonly used in classification and prediction models. One of them, model accuracy (also referred to as success rate), can be defined as the percentage of correctly predicted by the model, so it is sometimes considered the equivalent of the R^2 statistic. The positive predictive value is the percentage of true positives (TP) in the total positive predictions (TP+FP) or the proportion of affected area correctly modeled.On the contrary, the negative predictive value is the percentage of true negatives (TP) in the total negative predictions (TN +FN) or the proportion of unaffected areas correctly modeled.
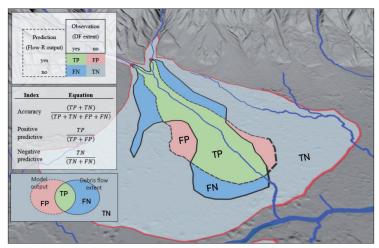

Figure 6. Classification and model performance evaluation according to the confession matrix method by Begueria (2006).

RESULT AND DISCUSSION

Best-fit calibration parameters

The parameter values of each event were based on the bestfit between the Flow-R model output and the observation extent (**Table 2**). These results were obtained by using the back analysis method to adjust the parameter values until the output matches the observed debris flow extent as closely as possible. The value of exponent x was adjusted to control the flow divergence. The spreading direction for x approach to 1 such as Bangga Village ($x = 4$) was the same as the multiple flow direction. When x increases such as in Poi Village ($x = 50$) the divergence decreases until it reaches zero, resulting in a single flow direction. To ensure that realistic velocities were not exceeded, a velocity threshold v_{lim} was used, resulting in more realistic run-out distances. The angle formed by the line connecting the source area to the farthest point reached by the mass movement is based on a minimum travel angle. Values close to zero, such as those found in Bangga ($TA = 2°$) and Poi ($TA = 2°$) Villages, indicate that mass flow movement is occurring further away than in Salua Village ($TA = 5°$), it shows a proportional relationship between TA with the length of debris flow.

Table 2. The parameter values of the Flow-R model output

No.	Debris flow events	Watershed	Calibration of Flow-R				Length of document-ed debris extent (km)
			Lateral spreading		Friction model		
			dh (m)	x	TA (°)	v_{lim} (m/s)	
1	Poi, Dolo Selatan	W23	1	50	2	15	1.2
2	Bangga, Dolo Selatan	W31	4	4	2	36	2.3
3	Salua, Kulawi	E35	1	20	5	40	0.6

Table 3. Watershed characteristicsi.emain channel elevation, length, slope, and size of a watershed

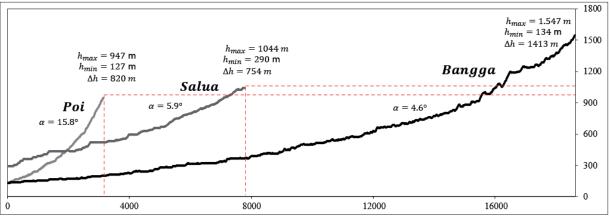| No. | Village | Main Channel | | | Length (km) | Slope (°) | Size (km²) |
		Elevation					
		Min	Max	Range			
1	Poi, Dolo Selatan	127	947	820	2.9	15.8	2.4
2	Bangga, Dolo Selatan	134	1547	1413	17.5	4.6	68.8
3	Salua, Kulawi	290	1044	754	7.3	5.9	14.4

Figure 7. Characteristic of the main channel in the studied area

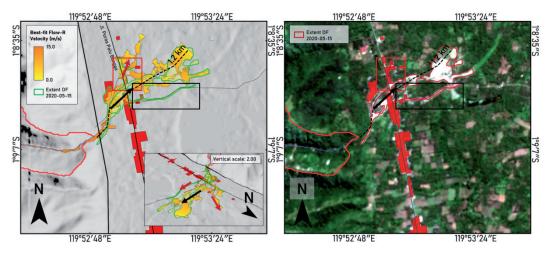**Figure 7** shows the different characteristics of the three main rivers in the study area.

From **Tables 2 and 3**, the relationship between depositional characteristics and subwatershed can be seen. The steepness of the main river and the amount of landslide material cause long runout distances to reach 1.2 km. Due to the small area of the sub-basin, the small rain catchment area is a factor in the slow flow velocity produced (15 m/s) and causes the remaining landslide material upstream to not be fully landslide material at the same time it transforms into a debris flood. Although the main river in Bangga Village is the most gentle, due to the wide catchment of rain and massive landslides upstream, it causes the longest runout distance. Then, the limited deposition area becomes a factor that causes the runout distance in Salua Village to be the shortest. However, the presence of settlements in the deposition area caused the case of debris flood in Salua Village to be interesting to study.

Evaluation of debrisflood extents

In general, the run-out model of Flow-R appears to fit with the observed debris flow extent (**Figure 8**). Similar to the previous study conducted by Fischer et al. (2016), the modeled flow path is reasonable and fits the observed debris flow extent.

However, Poi Village (W23) and Bangga Village (W31) show a mismatch between the model and observed flow extent. Overprediction was found in the northern part of the Poi Village and the southern part of the Bangga Village. It occurs because there are settlements in Poi Village and a road in Bangga Village (red rectangular in **Figure 8**), causing the debris flow path to not going through in that direction. Because the mass energy was converted on the incorrect path (red arrow in **Figure 8**), the path error causes underprediction models (black rectangular in **Figure 8**) in the southern part of Poi Village and the northern part of Bangga Village. Eventhough the path in SaluaVillage is correctly delineated, the accuracy value of Salua Village is lower than in Poi Village due to the limited deposition area, making the accuracy value and index calculation more sensitive.

The primary cause of the mismatch between the model and the observed debris flow extent is the use of DEMNAS data for topographic input data, which results in an error in the debris flow path, as illustrated by the red arrow (**Figure 9**). Digital Elevation Model (DEM), Digital Surface Model (DSM), and Digital Terrain Model (DTM) are the three most often used geospatial features created by UAV mapping systems. DEMNAS is categorized into DEM types that represent the bare-Earth surface after removing all natural and built features. This prevents the flow direction from being blocked or deflected by natural and built features of the environment.
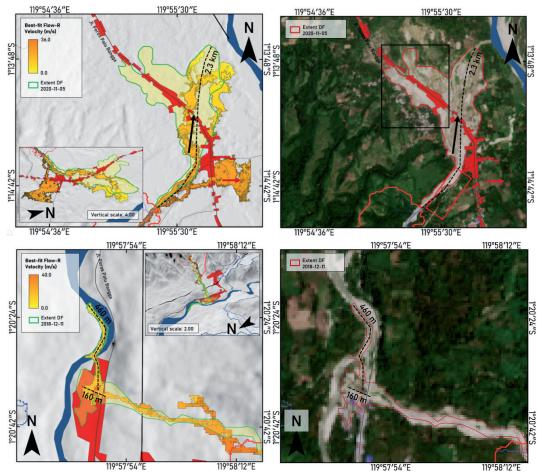
Figure 8. Best-fit debris flowsmodeling results of Flow-R for after the 28 September 2018 Palu Earthquake in the Poi, Bangga, and Salua Villages.

Quantitative analysis of modeling results based on calculations adopted from Beguería (2006) showed high variabilityin the accuracy, positive predictive value, and negative predictive value (**Figure 9**). Due to the largedeposition area and well-predicted unaffected region, the accuracy value in Poi and Bangga Villages is good (> 65), implying that the TN value has a major impact than others on the models (**Figure 10**).

Figure 9. Accuracy, positive predictive value, and negative predictive value index for best-fit Flow-R model output.

Figure 10. Classification between model and observed extent area according to Beguería (2006).

The large area of deposition and the high accuracy of the model predict the depositional path as factors that cause high True Negative (TN) values in Poi Village and Bangga Village (**Figure 10**). The significance of the TN value compared to the other classes is because of the high value of accuracy and negative prediction in the studied area.

CONCLUSION

Local debris flows modeling on Flow R was evaluated with three well-documented debris flow events on the break slopes on the west and east sides of the Palu Valley. Quantitative analysis was carried out in this study to assess the accuracy, positive predictive value, and negative predictive value of models. The result shows the individual back-analysis model of debris flows found good agreement between debris-flow paths predicted and documented debris flow path extent, although the parameters for rheological properties and erosion rate required in the software are limited.

The modeling of the debris flow path is not perfectly accurate and there is a mismatch between the model and the observed debris flow path due to the use of DEMNAS data for topographic input data, which results in an error in the debris flow path model. Digital Elevation Model (DEM), Digital Surface Model (DSM), and Digital Terrain Model (DTM) are the three most often used geospatial features created by UAV mapping systems. DEMNAS is categorized into DEM types that represent the bare-earth surface after removing all natural and built features. This prevents the flow direction from being blocked or deflected by natural and built features of the environment.

The quantitative analysis shows accuracy, positive predictive value, and negative predictive value, which varies considerably. Therefore, Flow-R is not suitable for complete hazard mapping but provides direct information about possible run-out debris flow paths. Furthermore, lateral spreading and friction of Flow-R model results can be used to calibrate process with rheological properties and erosion rate in other numerical modeling software, either for forward or back analysis.

REFERENCES

Ariza, A., Davila, N., 2021. Landslide Detection for Rapid Mapping Using Sentinel 2 [WWW Document]. URL https://github.com/sentinel-hub/custom-scripts/blob/master/sentinel-2/landslide_detection_rapid_mapping/README.md (accessed 6.5.22).

Beguería, S., 2006. Validation and evaluation of predictive models in hazard assessment and risk management. Nat. Hazards 37, 315–329. https://doi.org/10.1007/s11069-005-5182-6

Bellier, O., Sébrier, M., Seward, D., Beaudouin, T., Villeneuve, M., Putranto, E., 2006. Fission track and fault kinematics analyses for new insight into the Late Cenozoic tectonic regime changes in West-Central Sulawesi (Indonesia). Tectonophysics 413, 201–220. https://doi.org/10.1016/j.tecto.2005.10.036

Bellier, O., Siame, L., Beaudouin, T., Villeneuve, M., Braucher, R., 2001. High slip rate for a low seismicity along the Palu-Koro active fault in Central Sulawesi (Indonesia). Terra Nov. 13, 463–470. https://doi.org/10.1046/j.1365-3121.2001.00382.x

Fischer, F. Von, Keiler, M., Zimmermann, M., 2016. Modelling of individual debris flows using Flow-R : A case study in four Swiss torrents. 13th Congr. Interpraevent 2016, Lucerne, Switz. 257–264.

Holmgren, P., 1994. Multiple flow direction algorithms for runoff modelling in grid based elevation models: An empirical evaluation. Hydrol. Process. 8, 327–334. https://doi.org/10.1002/hyp.3360080405

Ishizuka, T., Kaji, A., Morita, K., Mori, T., Chiba, M., Kashiwabara, Y., Yoshino, K., Uchida, T., Mizuyama, T., 2017. Analysis for a Landslide Dam Outburst Flood in Ambon Island, Indonesia. Int. J. Eros. Control Eng. 10, 32–38. https://doi.org/10.13101/ijece.10.32

Larsen, M.C., Wieczorek, G.F., Eaton, L.S., Torres-Sierra, H., 2001. Natural Hazards on Aluvial Fans: The Debris Flow and Flash flood disaster of December 1999, Vargas State, Venezuela. Proc. Sixth Caribb. Islands Water Resour. Congr. 00965, 1–7.

Natawidjaja, D.H., Daryono, M.R., Prasetya, G., Udrekh, Liu, P.L.F., Hananto, N.D., Kongko, W., Triyoso, W., Puji, A.R., Meilano, I., Gunawan, E., Supendi, P., Pamumpuni, A., Irsyam, M., Faizal, L., Hidayati, S., Sapiie, B., Kusuma, M.A., Tawil, S., 2021. The 2018 Mw7.5 Palu "supershear" earthquake ruptures geological fault's multisegment separated by

large bends: Results from integrating field measurements, LiDAR, swath bathymetry and seismic-reflection data. Geophys. J. Int. 224, 985–1002. https://doi.org/10.1093/gji/ggaa498

National Agency for Disaster Management, 2021. Data Informasi Bencana Kabupaten Sigi [WWW Document]. URL http://pusdalops-bpbdsulteng.com/c_utama_auth/data_info_bencana/P321010 (accessed 3.30.21).

Patria, A., Putra, P.S., 2020. Development of the Palu–Koro Fault in NW Palu Valley, Indonesia. Geosci. Lett. 7, 1–11. https://doi.org/10.1186/s40562-020-0150-2

Perla, R., Cheng, T.T., McClung, D.M., 1980. A two-parameter model of snow-avalanche motion. J. Glaciol. 26, 197–207.

Quinn, P., Beven, K., Chevallier, P., Planchon, O., 1991. The prediction of hillslope flow paths for distributed hydrological modelling using digital terrain models. Hydrol. Process. 5, 59–79. https://doi.org/10.1002/hyp.3360050106

Simandjuntak, T.O., Surono, Supandjono, J.B., 1997. Geological Map of The Poso Quadrangle, Sulawesi.

Socquet, A., Simons, W., Vigny, C., McCaffrey, R., Subarya, C., Sarsito, D., Ambrosius, B., Spakman, W., 2006. Microblock rotations and fault coupling in SE Asia triple junction (Sulawesi, Indonesia) from GPS and earthquake slip vector data. J. Geophys. Res. Solid Earth 111, 1–15. https://doi.org/10.1029/2005JB003963

Sukamto, R.A.B., Sumadirdja, H., Suptandar, T., Hardjoprawiro, S., Sudana, D., 1973. Reconnaissance Geological Map of The Palu Quadrangle, Sulawesi.

Sukatja, C.B., Banata, W.R., Bahri, P., 2021. Mitigasi dan penanggulangan bencana banjir debris pasca gempa Palu 2018. J. Tek. Hidraul. 12, 25–38.

Sukido, Sukarna, D., Sutisna, K., 1993. Geological Map of The Pasangkayu Quadrangle, Sulawesi.

USGS, 2018. Earthquake Hazards Program M 7.5-72 km N of Palu, Indonesia [WWW Document]. URL https://earthquake.usgs.gov/earthquakes/eventpage/us1000h3p4/executive (accessed 1.23.22).

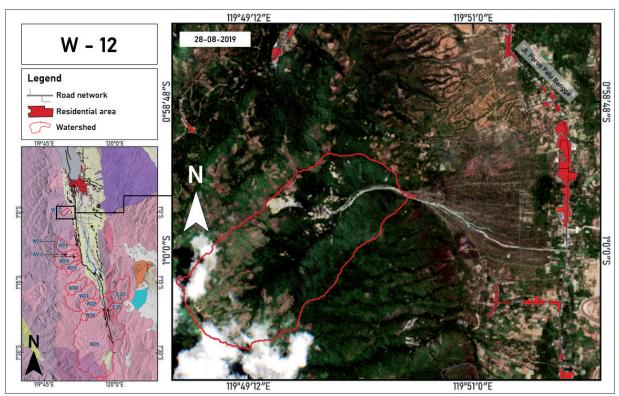Voellmy, A., 1955. Über die Zerstörungskraft von Lawinen (in German). Schweizerische Bauzeitung 73, 212–285.

Figure S1. Watershed condition W-12 with massive landslide in upstream after Palu Earthquake 28 September 2018
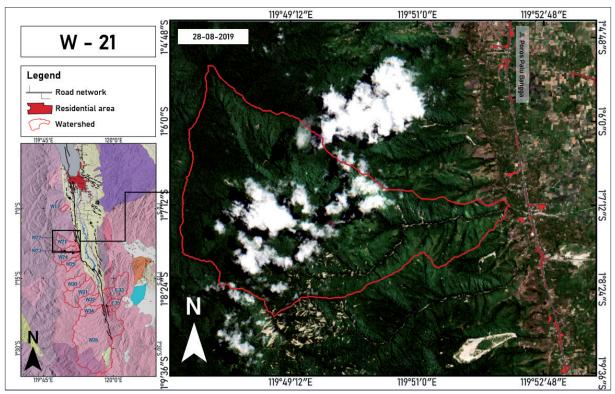

Figure S2. Watershed condition W-21 with massive landslide in upstream after Palu Earthquake 28 September 2018
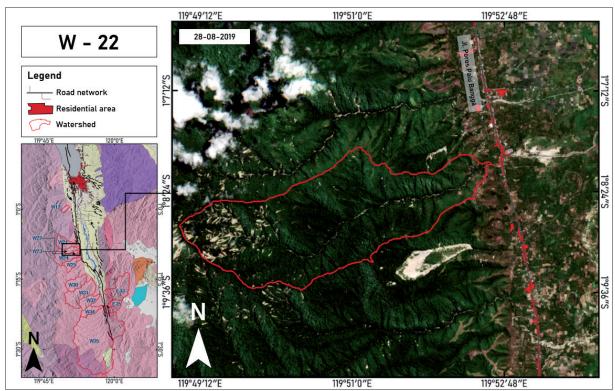
Figure S3. Watershed condition W-22 with massive landslide in upstream after Palu Earthquake 28 September 2018
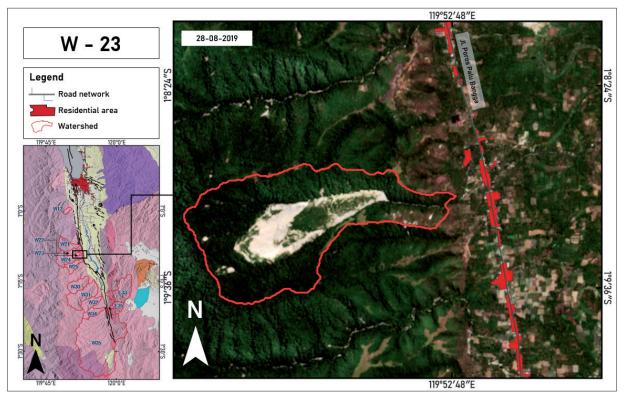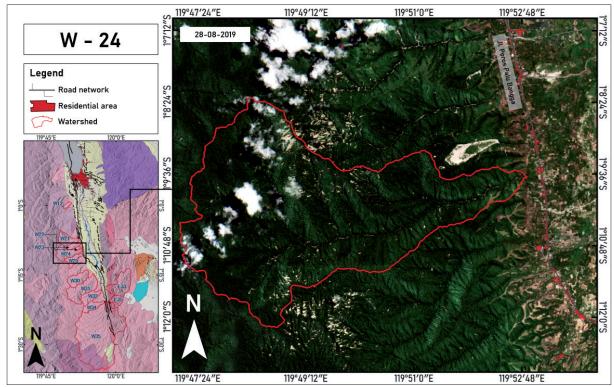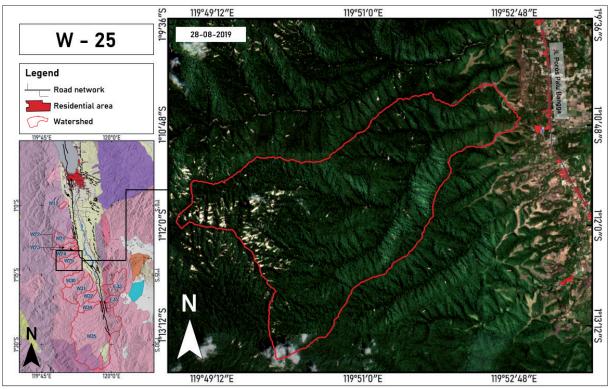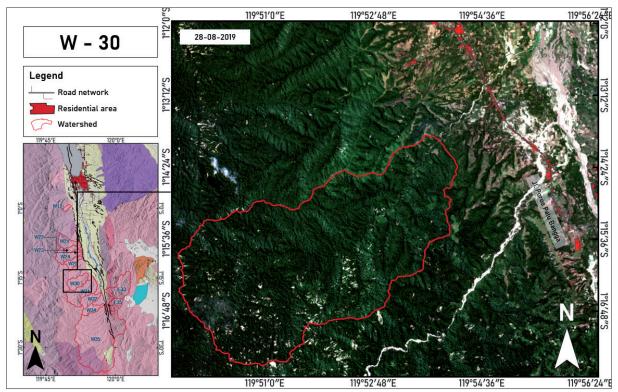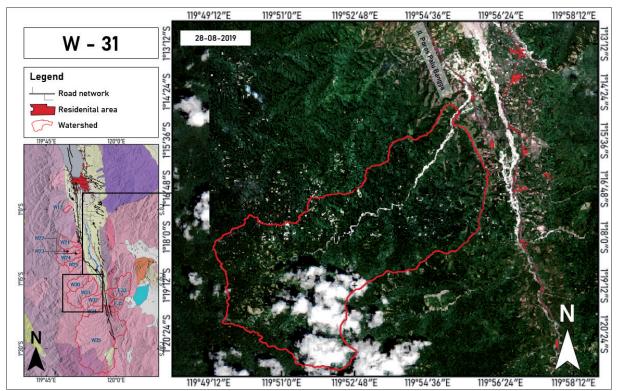

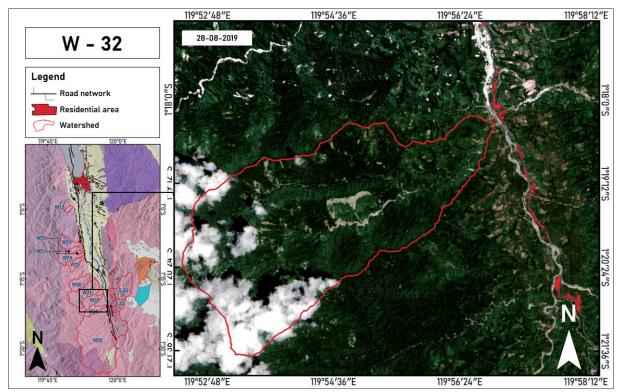**Figure S4.** Watershed condition W-23 with massive landslide in upstream after Palu Earthquake 28 September 2018

Figure S5. Watershed condition W-24 with massive landslide in upstream after Palu Earthquake 28 September 2018

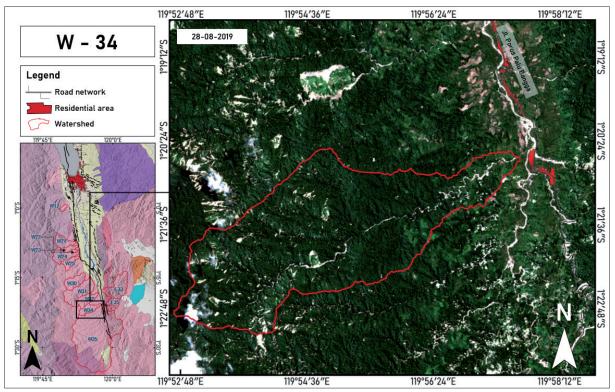**Figure S6.** Watershed condition W-25 with massive landslide in upstream after Palu Earthquake 28 September 2018

Figure S7. Watershed condition W-30 with massive landslide in upstream after Palu Earthquake 28 September 2018

Figure S8. Watershed condition W-31 with massive landslide in upstream after Palu Earthquake 28 September 2018

Figure S9. Watershed condition W-32 with massive landslide in upstream after Palu Earthquake 28 September 2018

Figure S10. Watershed condition W-34 with massive landslide in upstream after Palu Earthquake 28 September 2018
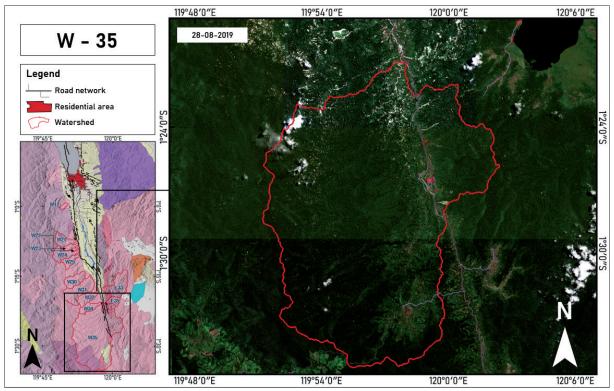
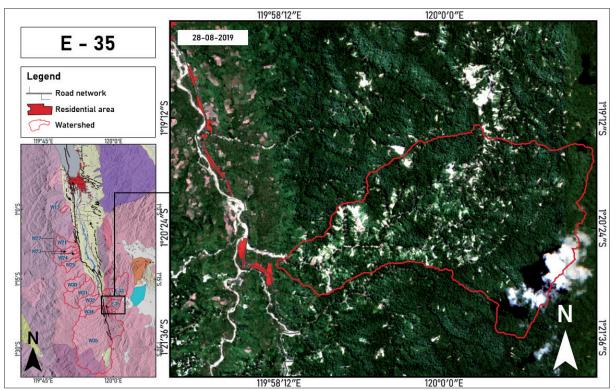**Figure S11.** Watershed condition W-35 with massive landslide in upstream after Palu Earthquake 28 September 2018

Figure S12. Watershed condition E-35 with massive landslide in upstream after Palu Earthquake 28 September 2018
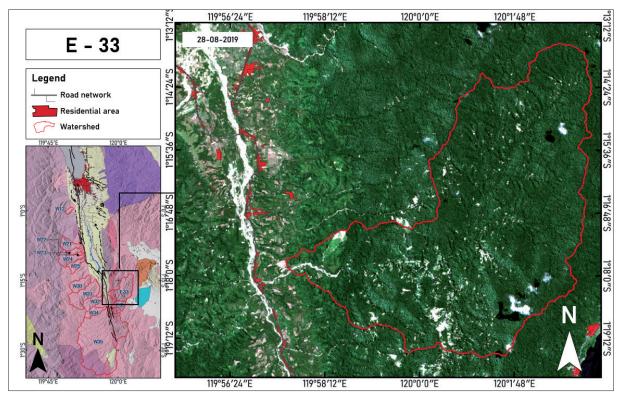
Figure S13. Watershed condition E-33 with massive landslide in upstream after Palu Earthquake 28 September 2018